Case Studies in Thermal Engineering 87 (2026) 108607

Contents lists available at ScienceDirect

Case Studies in Thermal Engineering

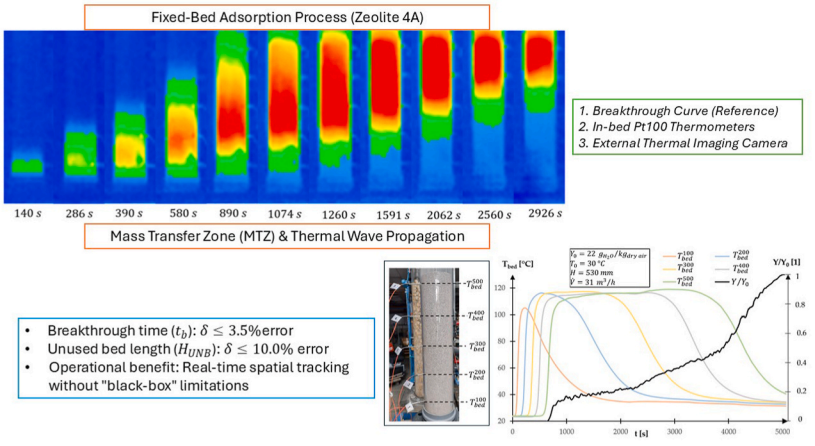
journal homepage: www.elsevier.com/locate/csite

Methods for tracking the mass transfer zone during fixed bed adsorption process

Levente Sor, Tibor Poós *

Department of Building Services and Process Engineering, Faculty of Mechanical Engineering, Budapest University of Technology and Economics, Műegyetem rakpart 3., Budapest, H-1111, Hungary

GRAPHICAL ABSTRACT



ARTICLE INFO

Keywords:
Thermal imaging camera
Zeolite
Mass transfer zone
Breakthrough point

ABSTRACT

This paper aims to show, how the movement of the mass transfer zone can be tracked during an adiabatic fixed bed adsorption process. During our measurements water vapor was adsorbed from saturated air on a fixed zeolite bed. Thermal imaging camera and resistance thermometers were used to track the movement of the mass transfer zone along the bed. Both methods are based on the fact that adsorption is exothermic. The heat generated during the process makes it possible to track the process following the change in bed temperature. From the heat effects the breakthrough point and the unused bed length can be calculated, which are both important parameters

* Corresponding author.
E-mail address: poos.tibor@gpk.bme.hu (T. Poós).

https://doi.org/10.1016/j.csite.2026.108607
Received 10 June 2026; Received in revised form 20 September 2026; Accepted 4 October 2026
Available online 9 October 2026
2214-157X/© 2026 The Authors. Published by Elsevier Ltd. This is an open access article under the CC BY license (http://creativecommons.org/licenses/by/4.0/).

of the process. These parameters can also be calculated from the breakthrough curve which is a method based on outlet gas flow measurement. The values obtained with thermal imaging camera and with built-in thermometers were compared to the values from the breakthrough curve. The breakthrough time had a maximum relative error of 2.6% in case of the thermometers and maximum 3.5% measured with the thermal imaging camera. In case of the unused bed length, a maximum relative error of 10% and 9.2% was observed with the two different thermal methods.

1. Introduction

Adsorption refers to the binding of a substance to a solid surface. Among its industrial applications there is for example the reduction the moisture content of air, removing of hydrogen sulphide from gases, and the capture odours. There are also applications where the separation of gas stream components is achieved, such as the separation of air using pressure-swing adsorption [1].

A process which becomes more and more important in our century is the carbon capture technology, where the removal of CO_2 is performed from an exhaust gas stream [2].

This is not just an old, robust technology but it is still an intensively researched field as well. Adsorption desalination for example is a new, emerging method for producing drinking water from sea water while using waste heat from industrial processes [3]. The method also produces cold energy as a byproduct, which is particularly useful.

Most common type of adsorbents used today are different types of zeolite [4], silica gel [5] and activated charcoal [2].

Most of the time adsorption is a semi-continous operation where at least two parallel fixed bed columns operating in adsorption-desorption cycles [5].It is crucial for the operator of the adsorption process to know exactly, when to switch between the columns. Thus it is important to measure somehow, when does the column reaches its full capacity. Most of the time it is done by measuring the outlet concentration. The problem with this method is that the process is treated as a “black box”, the operator does not know, how much free capacity the adsorber has at a given time. It can only be decided, if the adsorption process is measured exactly where it takes place: in the adsorbent bed. The aim of this paper is to present two useful methods with which it is possible to track the process at any given time, thus enabling the quick modification of operating parameters during the process if needed.

2. Equipment and methods

2.1. Adsorption zone in a fixed bed adsorber column

In case of a fixed bed adsorption processes, plotting the ratio of the outlet and inlet concentrations as a function of elapsed time yields the breakthrough curve [6].

The adsorption zone is the active, "working" layer in the column where substance binding is currently taking place; the process has not yet begun above it and has already ended under it. As long as the adsorption zone is within the column, the outlet concentration is ideally zero. As it reaches the end of the column, the concentration in the outlet gas stream begins to change rapidly. When the outlet concentration reaches 5% of the feed concentration ($C/C_0 = 0.05$), the system reached the breakthrough point. The elapsed time, when the breakthrough occurs (t_b) is an important operating parameter [7]. Afterwards, the adsorption zone gradually leaves the column, and the concentration of the adsorbate in the outlet flow continuously increases. If $C/C_0 = 0.95$ is reached, the adsorption zone has practically left the bed entirely [7], [8]. However, equilibrium is only fully established after an infinite amount of time, at which point the outlet concentration is equal to the inlet concentration ($C/C_0 = 1$).

In practice, when $C/C_0 = 0.95$, we consider equilibrium to have been reached, since it is not possible to wait indefinitely for equilibrium to be established. Furthermore, concentration measurements are subject to error, so we would never obtain an exact, constant value.

The mass balance for the unit cross-sectional area of the entire bed can be expressed by the following equation in the case of a

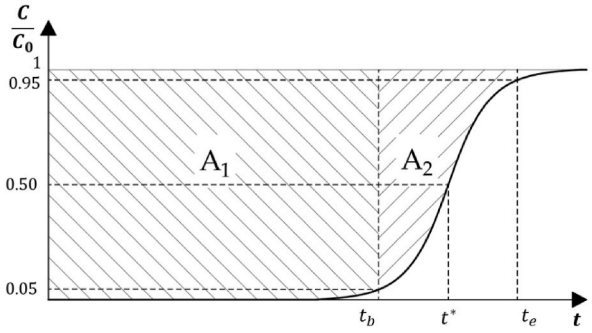


Fig. 1. Breakthrough curve of an adsorber
(A_1: Area between breakthrough curve and $C/C_0 = 1$ from 0 to t_b.; A_2: Area between breakthrough curve and $C/C_0 = 1$ from t_b to t_e).

vertical breakthrough curve (infinitely short adsorption zone) [9]:

$$v_0 C_0 t^* = H\rho_{bulk}\left(X_{eq} - X_0\right) . \tag{1}$$

If the adsorption isotherm is available, the value of X_{eq} can be obtained from it, while X_0 is either determined by measurement or, if the process starts with a fully regenerated adsorbent, then $X_0 \cong 0$. By entering the feed data, Equation (1) can be used to calculate the amount of adsorbate bound during the entire process, as well as the time t^* required to reach equilibrium. It should be noted that this value is strictly theoretical, since mass transfer is never perfect. There will always be an unused bed segment at the end of the column, since the process is stopped at breakthrough.

If the adsorption isotherm is not available, the amount of adsorbate bound can also be calculated from the breakthrough curve. The area between the breakthrough curve and $C/C_0 = 1$ line gives the t^* time, which is obtained by integration (Equation(2)) [6]. This area is the sum of the area A_1 and A_2 on Fig. 1 [9], [10].

$$t^* = \int_{t=0}^{t=t_e} \left(1 - \frac{C}{C_0}\right) dt \tag{2}$$

If the breakthrough curve is symmetric, it corresponds to the time at which the breakthrough curve reaches the value $C/C_0 = 0.5$, as shown in Fig. 1. The t^* is proportional to the full capacity of the bed according to Equation (1). If t^* is multiplied by the mass flow density $v_0 C_0$ and the cross-sectional area A, the idealized charge capacity is obtained in kg_{ads}.

The same integration until the t_b breakthough time results in t_u, which is proportional to the useful capacity of the bed. (A_1 area on Fig. 1) [6]:

$$t_u = \int_{t=0}^{t=t_b} \left(1 - \frac{C}{C_0}\right) dt . \tag{3}$$

If t_u is multiplied by the mass flow density $v_0 C_0$ and the cross-sectional area A, the real charge capacity is obtained in kg_{ads}. Given t^* and t_u the length of the unused bed can be expressed as [9]:

$$H_{UNB} = \left(1 - \frac{t_u}{t^*}\right)\mathrm{H} . \tag{4}$$

The velocity of the propagation of the concentration front in the bed can be expressed by the following equation [9], [11]:

$$v_{front} = \frac{v_{gas}}{\left[1 + \left(\frac{1-\varepsilon}{\varepsilon}\right)\left(\frac{X_{eq}}{C_0}\right)\right]} . \tag{5}$$

This equation holds true if we assume that mass transfer resistances are negligible during adsorption, that axial mixing and gas-phase diffusion are negligible, and that the adsorption is isothermal and the adsorption isotherm is linear.

Due to the exothermic nature of adsorption, the propagation of the adsorption zone in an adiabatic process results in a gradual increase in temperature along the length of the bed. However, the rate at which the resulting temperature front propagates is not necessarily equal to the velocity of the adsorption zone. The rate of propagation of the temperature front can be expressed as [11], [12]:

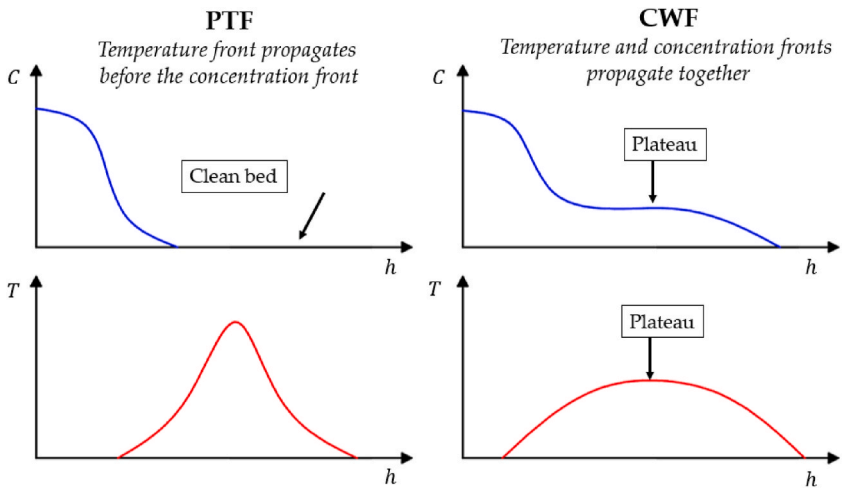


Fig. 2. PTF and CWF fronts in case of adsorption (based on [12]).

$$v_{temp} = \frac{v_{gas}}{\left[1 + \left(\frac{1-\varepsilon}{\varepsilon}\right)\left(\frac{c_{p,ads}}{c_{p,gas}}\right)\right]} . \tag{6}$$

In an adiabatic process, two types of adsorption zones can form, depending on whether the temperature front or the concentration front propagates faster: Pure Thermal Front (PTF); or Combined Wave Front (CWF). In case of PTF the temperature front propagates faster than the concentration front, because $v_{temp} > v_{front}$. In this case, the adsorption takes place nearly at feed temperature, it can be considered as isotherm. In case of CWF, the concentration front propagates faster because $v_{temp} < v_{front}$. The temperature front travelling behind the concentration front heats up the gas phase before it reaches the adsorption zone. The rise in temperature is not favourable for adsorption; thus the adsorption zone becomes wider, and a combined temperature-concentration front (CWF) forms. In this case, the breakthrough time is shortened, the breakthrough curve becomes less steep, and the length of the unused bed also increases [12]. Fig. 2 shows the two different cases.

In most cases, the velocity of concentration fronts cannot be calculated analytically, since the approximations discussed above cannot be applied, or certain parameters are unknown. However, it is possible to compare the speeds of the temperature and concentration fronts using the ratios X_{eq}/C_0 and $c_{p,ads}/c_{p,air}$ since these ratios are the primary factors influencing the speed at which the fronts propagate. If the following condition is true, then the concentration front moves faster than the temperature front [12]:

$$\frac{X_{eq}}{C_0} < \frac{c_{p,ads}}{c_{p,gas}} . \tag{7}$$

If the condition (7) is met, a CWF is formed; if it is not met, a PTF may be formed. In the latter case, condition (8) needs to be examined as well [12].

$$\frac{X_{eq}^{T_{bed,max}}}{C_0} > \frac{c_{p,ads}}{c_{p,gas}} . \tag{8}$$

If condition (8) is met, PTF is formed, if it is not met, it is not possible to determine whether CWF or PTF will develop based solely on operational parameters and material properties. Table 1 shows the possible cases presented.

As part of our research, a measuring equipment was built that first humidifies the ambient air and then captures the water vapor from the humidified air through adsorption. The instrumentation allows us to monitor the thermal processes associated with adsorption.

2.2. Description of the measuring equipment

The P&ID of the measuring equipment used for the adsorption measurements is shown on Fig. 3.

The main elements of the system are the C-102 blower, the T-201 absorber column and the T-202 adsorber column. The C-102 blower supplies ambient air to the bottom of the absorber, where tap water is sprayed from the top, in counterflow. As a result of the heat and mass transfer that takes place in the absorber, the air exiting at the top of the tower becomes nearly saturated with water vapour, which is then directed to the inlet of the adsorber column. As the air passes through the adsorbent particles, its moisture content decreases. This decrease could be monitored using the ALMEMO D6 FHAD 36 Rx digital temperature and humidity meter installed in the outlet pipe. We used LTE-A zeolite as adsorbent, which can be expressed as $Na_{12}(Al_{12}Si_{12}O_{48}) \cdot 27H_2O$. The zeolite particles are nearly spherical, with a characteristic diameter of $2 \pm 0.3\ mm$. The construction material of the T-202 adsorber column is PMMA. The main dimensions of the column are shown in Table 2.

Pt100 resistance thermometers were installed to monitor the adsorption zone, spaced 100 mm apart, as indicated by the TR-202 in Fig. 3 The thermometers extend to the centre of the bed and measure its temperature at a specific height. A moisture content meter (XR-203, TR-203) has been installed in the outlet pipe, which allows the recording of the breakthrough curve. The temperature of the air entering the adsorber is measured by a TR-201 resistance thermometer. The sensors are connected to an ALMEMO data logger. The measured values are recorded by the Apollo module of the IMPERIUM Laboratory Information System [13], in which the sampling rate was 10 *s*. A Testo 881-3 thermal imaging camera was also used to monitor the adsorption zone. The thermal imaging camera was mounted on a tripod and positioned so that the entire adsorbent bed was visible in the image.

Table 1
Changes in temperature and concentration profiles as a function of specific conditions [7].

	$\frac{X_{eq}^{T_{bed,max}}}{C_0} > \frac{c_{p,ads}}{c_{p,gas}}$	$\frac{X_{eq}^{T_{bed,max}}}{C_0} < \frac{c_{p,ads}}{c_{p,gas}}$
$\frac{X_{eq}}{C_0} < \frac{c_{p,ads}}{c_{p,gas}}$	CWF	CWF
$\frac{X_{eq}}{C_0} > \frac{c_{p,ads}}{c_{p,gas}}$	PTF	CWF or PTF

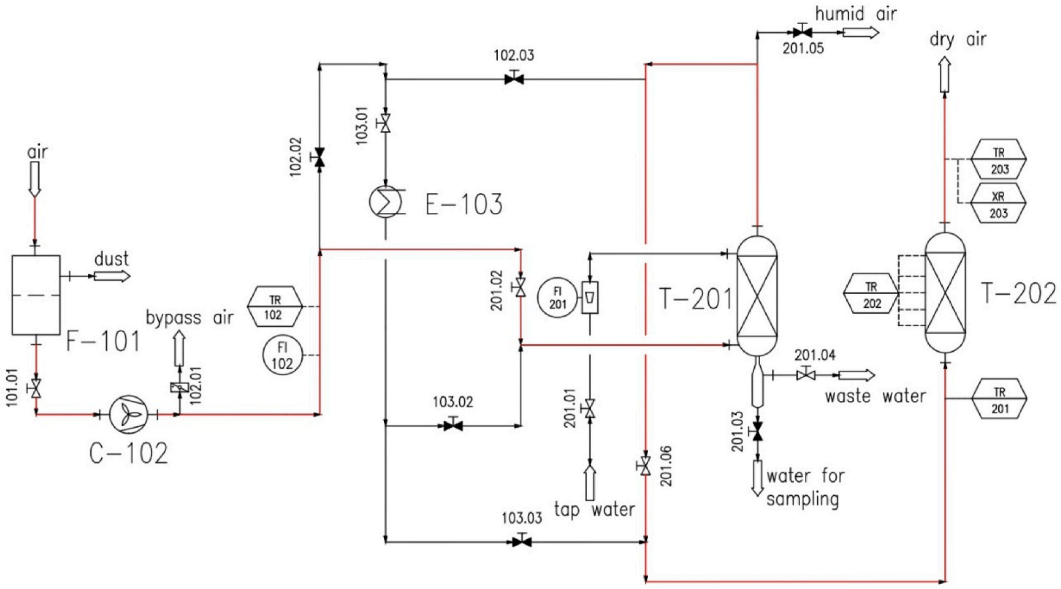


Fig. 3. P&ID of the measuring equipment.

Table 2
Main dimensions of the adsorber column

Dimension	Value [*mm*]
Height	1000
Outer diameter	110
Wall thickness	5
Height of the bed	*max.* 900

2.3. Method of measurement

As the first step of the measurement, the zeolite was dried in a drying oven at 180°*C* and atmospheric pressure for at least 24 hours. It was then loaded into the adsorber using a funnel. After loading the bed, the support grid was placed on top. Next, the thermometers were positioned along the length of the bed. Fig. 4 shows the adsorber ready for measurement, with the absorber supplying humid air visible in the background.

Finally, all the sensors were connected to the data collector and the data collector to a PC.

After the assembly, feeding of tap water to the absorber was started. After about 5 min, the entire absorber had reached the temperature of the water, at which point the C-102 blower was switched on to provide airflow through the system. This can be considered the start of the measurement so at this point $t = 0$. During the measurement, it was necessary to adjust the volumetric flow rate using butterfly valve 102.01. The more butterfly valve 102.01 was opened, the lower the air flow into the absorber was. The volumetric flow rate could be calculated using the pressure difference across the FI-102 orifice flange. To calculate the volumetric flow rate, the temperature of the ambient air flowing through the orifice flange was also required, which was measured by the TR-102 thermocouple.

By adjusting the volumetric flow rate of the water accordingly, flooding of the absorber can be prevented. The adjustment was performed using the FI-201 rotameter.

By varying the temperature of the water sprayed into the absorber, the temperature of the air entering the adsorber (T_0) can be controlled, as measured by the TR-201 thermometer. It can be summarized that the two controlled variables were the volumetric flow rate and the temperature of the air entering the adsorber. The modified variables connected to them were the status of the valves 102.01 and the temperature of the water. At the outlet, the rise of φ_{out} showed that the breakthrough had been reached. The measurement was stopped when $\varphi_{out} \cong const.$ and the bed cooled down below 50°*C* at its full length.

2.4. Evaluation methods

During the evaluation, it was necessary to determine the volumetric flow rate of the air flowing through the column, as well as the points on the breakthrough curve and the temperature of the bed as a function of elapsed time.



Fig. 4. The assembled measuring equipment.

2.4.1. Calculating the volumetric flow rate of air

Using a U tube manometer connected to the FI-102 orifice flange on its both sides, the differential pressure across the flange can be calculated from the differences in liquid level (ΔL_{H_2O}) with Equation (9):

$$\Delta p_{fl} = \rho_{H_2O} g \Delta L_{H_2O}, \tag{9}$$

where ρ_{H_2O} is the density of the measuring liquid (water) ($\sim 1000\ kg/m^3$), g is the standard gravity ($9.81\ m/s^2$).

The air temperature (T_{fl}) flowing through the orifice flange was recorded using the TR-102 thermocouple; which remained nearly constant throughout the measurement. Using this temperature and the ideal gas law, the density of the air was calculated as follows:

$$\rho_{air} = \frac{\overline{M}_{air} p_{air}}{R T_{fl}}, \tag{10}$$

where $\overline{M}_{air}$ is the average molar mass of air ($2.897 \cdot 10^{-2} kg/mol$), p_0 is the atmospheric pressure ($101325\ Pa$), R is the ideal mass constant ($8.314\ \frac{J}{kmol}$).

Next, the pressure drop across the flange can be calculated [14]:

$$\dot{V} = \alpha \varepsilon_{exp} \frac{d^2 \pi}{4} \sqrt{\frac{2\Delta p_{fl}}{\rho_{air}}}, \tag{11}$$

where α is a constant of the flange, in this specific system, its value was 0.62; ε_{exp} is the expansion number ≈ 1; d is the diameter of the flange, $0.025\ m$.

2.4.2. Plotting the breakthrough curve

During the measurement, the data logger recorded the outlet air temperature and relative humidity as a function of time. To plot the breakthrough curve, the time values first had to be corrected. To do this, it was necessary to subtract the time elapsed between the start of data collection and the start of the C-102 blower (t_{start}) from the measured t_{rec}, as well as the instrument's time constant (t_h). The latter was determined prior to the measurement by placing the instrument in a space with a higher humidity level, which can be considered as a unit-step disturbance. The time during which the value displayed by the instrument reached 63% of the equilibrium value can be considered the instrument's time constant [15]. For the instrument we used, this value was 33 s. The time t used to plot the

breakthrough curve was calculated using Equation (12):

$$t = t_{rec} - t_{start} - t_h \ . \tag{12}$$

To plot the breakthrough curve, the next step was to determine the absolute moisture content (Y) at each measurement point using the φ_{out} values recorded by the XR-203 and the T_{out} values recorded by the TR-203. To do this, it was first necessary to determine the water vapour pressure at equilibrium at the given temperature. In the operating temperature range of 20–60°C, the Buck equation provides the best solution for this [16]:

$$p^*_{H_2O} = 6.1121e^{\left(18{,}678-\frac{T_{out}}{234.5}\right)\left(\frac{T_{out}}{257.14+T_{out}}\right)} \ . \tag{13}$$

Given the equilibrium water pressure and relative humidity, the current water vapour pressure was calculated using the following equation:

$$p_{H_2O} = p^*_{H_2O}\,\varphi \ . \tag{14}$$

Using the ideal gas law, the absolute moisture content can be calculated for a water-air system:

$$Y = 0.622\frac{p_{H_2O}}{p_{air} - p_{H_2O}} \ . \tag{15}$$

The Y values were calculated at every t time stamp for the outlet. However, the $t - Y$ data series was subject to significant noise, so it was necessary to apply smoothening. For this purpose, Savitzky-Golay smoothening was used. The method we used was based on a fourth-degree polynomial with a window width of 7. Accordingly, the smoothened values in point i can be calculated using the following equation [17]:

$$Y^s_i = -2Y_{i-3} + 3Y_{i-2} + 6Y_{i-1} + 7Y_i + 6Y_{i+1} + 3Y_{i+2} - 2Y_{i+3} \ . \tag{16}$$

For plotting the breakthrough curve, it was also necessary, to determine the inlet Y_0. The air exiting the T-201 absorber is saturated with water at the measurement temperature. This was checked with a relative humidity sensor at different air flow rates. However, between the instrument and the point of entry into the adsorber, some of this water vapor condensed on the pipe wall, as the ambient temperature was typically lower than the measurement temperature. For this reason, we observed that the outlet Y becomes constant after the adsorption process is complete, but even after a very long time, it does not reach the Y_0 measured near the adsorber inlet. For this reason, the constant outlet Y value after the adsoprtion process was considered as Y_0. By The breakthrough curve was obtained by plotting the $\frac{Y^s}{Y_0} - t$ data series.

2.4.3. Bed temperature as a function of time

While plotting the data series $T_{bed} - \mathrm{t}$, which was recorded with the 5 thermometers along the adsorption bed, it was necessary to correct the recorded t_{rec} time stamps with the t_{start} and t_h using Equation (12). The temperature measurement is not as noisy as the φ measurement, as a result applying smoothening was not necessary. The error of the thermometers relative to one another is only a few tenths of a degree $^\circ C$, which amounts to a deviation of less than 1% for the temperature differences under investigation. Therefore, we disregarded this error, and no further correction was necessary.

3. Results

The results are presented for a specific measurement, the operational parameters of which are listed in Table 3.

Given the specific material properties and operational parameters, it is possible in certain cases to determine the relative velocities of the concentration front and the temperature front (Equation (7) and (8)). The data necessary for determining the relative velocities are collected in Table 4.

The equilibrium moisture content of the adsorbent at the initial temperature was determined in a previous study, in which the adsorption and desorption isotherms of the zeolite we used were measured at 30; 40; 50, and 60°C [4]. Our measurement was performed at 30°C; therefore, given the initial concentration Y_0, ${X_{eq}}^{30^\circ C}$ can be obtained from the isotherm curve. The specific heat of zeolite was taken from the literature [18]. During the calculation of the specific heat of the gas phase, the moisture content was also

Table 3
Operational parameters of the presented measurement

Parameter	Value
$\dot{V}\,[m^3/h]$	31
$T_0[^\circ C]$	30
$Y_0\ \left[g_{H2O}/kg_{dry\ air}\right]$	22
Type of adsorbent	zeolite
$H\,[mm]$	530

Table 4
Data for calculating the velocities of the temperature and concentration fronts

Parameter	Value
$X_{eq}{}^{30^\circ C}\left[g_{H_2O}/kg_{dp}\right]$	35
$Y_0\left[g_{H_2O}/kg_{dry\ air}\right]$	22
$c_{p,ads}\ [J/kgK]$	935
$c_{p,gas}\ [J/kgK]$	1056

taken into account [19]:

$$c_{p,gas} = 1005 + 1.88Y_0 \tag{17}$$

The relative velocities can be checked by substituting the condition in Equation (7), which was discussed earlier. That means $\frac{35}{22} <> \frac{935}{1056}$, so $1.59 > 0.89$, as a result it is not fulfilled. If the condition in Equation (7) is fulfilled, the two fronts propagate together, CWF forms. In this case however, it is not fulfilled, so it is necessary to check the condition in Equation (8) [11], [12].

Fig. 5 shows the breakthrough curve for the current measurement and the T_{bed} temperatures measured at different heights as a function of time. It can be obtained that $T_{bed,max} = 118^\circ C$. Since the adsorption isotherm is not available at this elevated temperature, the value of $X_{eq}{}^{T_{bed,max}}$ is unknown. For this reason, examining the initial parameters alone did not allow us to determine what type of front was present in this specific case. However, by analysing the breakthrough curve and the $T_{bed} - t$, it was possible to conclude whether a PTF or a CWF formed.

The following signs indicate the formation of CWF.

- In Fig. 5, the breakthrough curve marked in black reveals a slowly rising "plateau" phase following the initial ramp-up phase, followed by another rapid rise until $Y/Y_0 = 1$, just like in the case of CWF in Fig. 2.
- In Fig. 5, high temperature plateaus can be observed on the bed temperature curves, which refer to the presence of CWF as well, just like in Fig. 2.
- The outlet airflow begins to warm up only when the concentration front arrives. If this were a PTF, the air temperature would have had to rise even before the breakthrough. The breakthrough curve and the outlet air temperature as a function of time are shown in Fig. 6.

The diagrams obtained during the measurement shows that, in this system, the concentration front and the temperature front move together.

The following section demonstrates how to calculate the breakthrough point and the length of the unused bed from the breakthrough curve, the built-in thermometers, and the thermal imaging camera recordings.

3.1. Evaluation of the breakthrough curve

The breakthrough curve recorded during the measurement and then smoothened is shown in Fig. 7, where the time values required to calculate the length of H_{UNB} are marked.

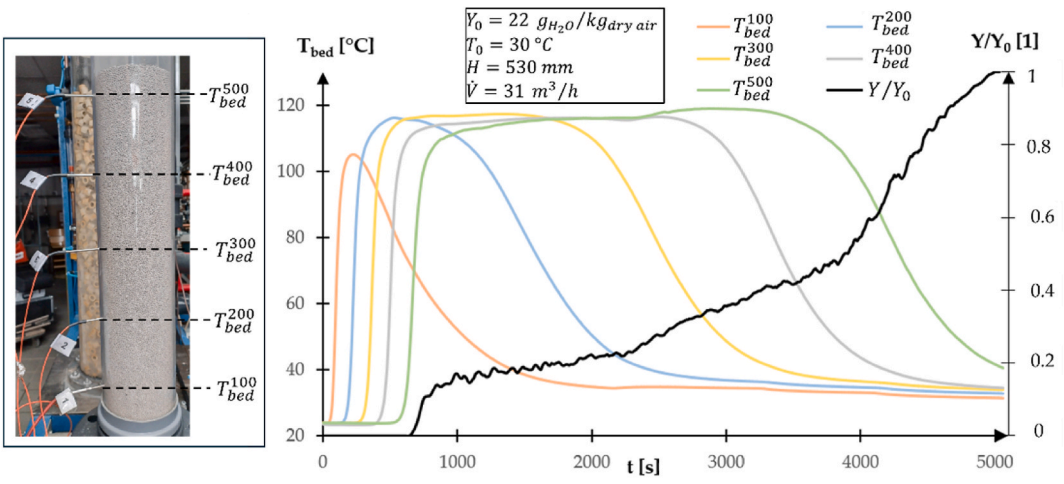


Fig. 5. Breakthrough curve and adsorbent bed temperature as a function of time.

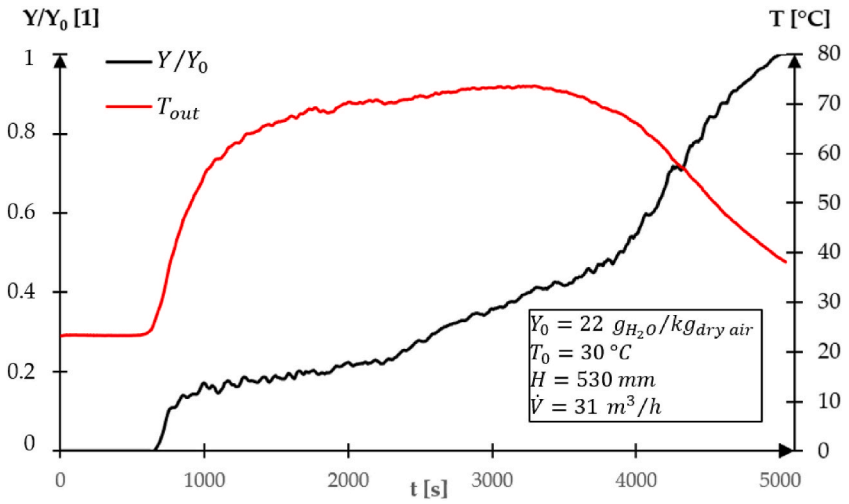


Fig. 6. Temperature of the outlet airflow as a function of time and the breakthrough curve.

Fig. 7 shows that the value of the breakthrough curve remained at zero throughout the period prior to breakthrough. As the concentration front reached the end of the bed, the outlet concentration began to rise rapidly. The t_b^{br} breakthrough point based on the breakthrough curve, was reached at 720 *s*, and the equilibrium point occurred at 4815 s.

Given the breakthrough curve, the length of the unused bed length can be calculated by performing two numerical integrations using the trapezoidal method:

$$\int_a^b f(t)dt \approx \frac{1}{2}\sum_{i=2}^{N}(t_i - t_{i-1})\left[\left(\frac{Y}{Y_0}\right)_i - \left(\frac{Y}{Y_0}\right)_{i-1}\right] \tag{18}$$

Using Equation (2) the t^* time was calculated, which is proportional to the full capacity of the bed. The integration limits were 0 s and 4815 *s*, thus t^* was calculated to be 3257 *s*. The t_u time, which is proportional to the useable capacity of the bed can be calculated with Equation (3). The integration limits were 0 s and 720 *s*, thus t_u was calculated to be 717 s. Given t^* and t_u, the height of unused bed can be calculated using Equation (4), which was 413 *mm* in this particular case. The calculation also confirms that the adsorption zone is relatively long compared to the total length of the bed, which is also typical for CWF.

An error propagation analysis was also conducted for the obtained parameters. The breakthrough time t_b^{br} exhibited an absolute uncertainty of ±9.4 s. Considering the uncertainty of the relative humidity sensor, its propagated effect on the numerically integrated H_{UNB}^{br} was negligible.

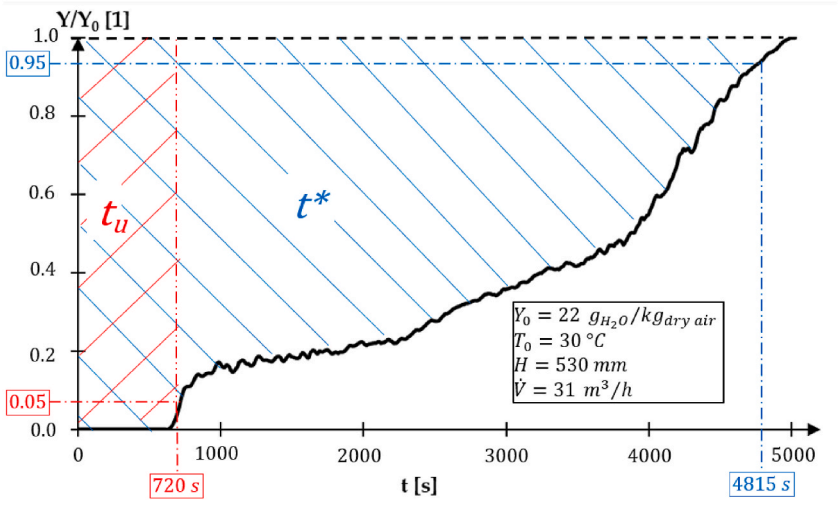


Fig. 7. Breakthrough curve and the areas to be calculated.

3.2. Evaluation of the thermometers built into the adsorbent bed

Fig. 5 also shows that, prior to the breakthrough, temperature increases occurred at nearly equal intervals on the thermocouples placed along the length of the bed. This makes it possible to calculate the velocity of the temperature front in each section, given the time elapsed between the rising segments appearing on two neighbouring thermometers and the distance between the two thermometers. In this case, the temperature front moves together with the concentration front; therefore, the resulting velocity is also the velocity of the adsorption zone. t_{front} represents the time at which the temperature at a given thermometer has increased by $5°C$ compared to the initial state. Five thermometers are placed along the length of the bed, which result five time values. For this measurement, these values are shown in the first row of Table 5, or can be obtained from Fig. 8. The time differences, which elapsed from the previous t_{front}, are shown in the second row of Table 5.

It can be seen that the value of Δt^{100}_{front} is significantly smaller than all the other. Due to this great difference, Δt^{100}_{front} was not considered during further evaluation. The Δh distance between two thermometers was uniformly 100 mm, thus given the individual Δt^{h}_{front} values, the velocity of the front could be calculated:

$$v^{h}_{front} = \frac{\Delta h}{\Delta t^{h}_{front}}. \tag{19}$$

The velocity value calculated at each h height is shown in Table 5. Averaging the velocities, $\overline{v}_{front} = 0.756\ mm/s$. Averaging can be performed because the zeolite adsorption isotherm is approximately linear at $30°C$ [4] over the range studied, from which it can be concluded that the concentration front propagates through the bed at a nearly constant velocity [9]. Using $\overline{v}_{front}$, the breakthrough time based on the thermometers could be calculated:

$$t^{tm}_{b} = \frac{H}{\overline{v}_{front}}. \tag{20}$$

Since the front had to travel a distance of $H = 530\ mm$, t^{tm}_{b} was equal to 705 s.

Fig. 5 shows that, based on the temperature plots, the temperature plateaus became progressively longer as one moved up the column, suggesting that the velocity at the end of the adsorption zone was lower than the velocity of the front. The method for calculating the speed at the front of the zone was described earlier; a similar principle was applied to the end of the zone as well. $50°C$ was chosen as a lower limit temperature. t_{tail} is the time, at which the temperature at a given thermometer decreases below $50°C$. The method for obtaining the t_{tail} values is presented on Fig. 9. The values for the present measurement are shown in Table 6.

The Δh distance between the thermometers is uniformly 100 mm in this case as well. The velocity of the trailing end can be calculated using a distance-time ratio according to the equation (21):

$$v^{h}_{tail} = \frac{\Delta h}{\Delta t^{h}_{tail}}. \tag{21}$$

The calculated velocity values for each thermometer are listed in Table 6. The velocities are averaged, $\overline{v}_{tail} = 0.110\ mm/\ s$.

Given $\overline{v}_{front}$ and $\overline{v}_{tail}$ velocities, the length of H^{tm}_{UNB} at breakthrough could be calculated. t^{tm}_{b} is calculated according to Equation (20). The distance travelled by the bottom of the zone during this time:

$$h_{tail} = \frac{H}{\overline{v}_{front}}\overline{v}_{tail}. \tag{22}$$

At the time of breakthrough, the bottom of the adsorption zone was lower than the height of the entire bed. The section between the bottom of the adsorption zone and the top of the bed is the unused bed section, the length of which can be calculated:

$$H^{tm}_{UNB} = H - h_{tail} = H - \frac{H}{\overline{v}_{front}}\overline{v}_{tail} = H\left(1 - \frac{\overline{v}_{tail}}{\overline{v}_{front}}\right) \tag{23}$$

Substituting the measured data into the equation, H^{tm}_{UNB} was found to be 453 mm.

Based on error propagation, $t_{b,tm}$ had an absolute uncertainty of ±4 s originating from sensor accuracy (±0.2°C). The resulting propagated error was similarly negligible for H^{tm}_{UNB}.

The smaller the difference between $\overline{v}_{front}$ and $\overline{v}_{tail}$, the closer the bottom and top of the zone can remain to each other, resulting in a shorter H^{tm}_{UNB}, which is advantageous from an operational standpoint. In the ideal case—where material transfer resistances, axial

Table 5
The time of the temperature increases along the bed

Parameter	100 mm	200 mm	300 mm	400 mm	500 mm
$t^{h}_{front}\,[s]$	72	193	326	459	603
$\Delta t^{h}_{front}\,[s]$	72	121	133	133	144
$v^{h}_{front}\,[mm/s]$	N/A	0.826	0.752	0.752	0.694

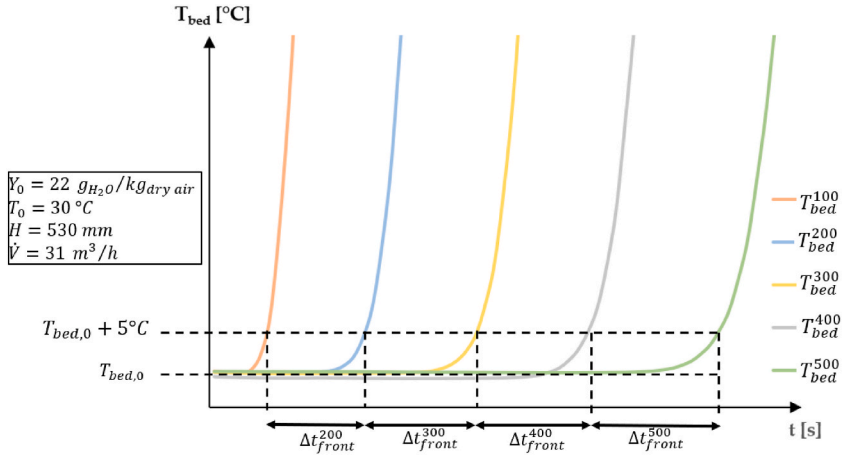


Fig. 8. Obtaining the time of the temperature increases along the bed.

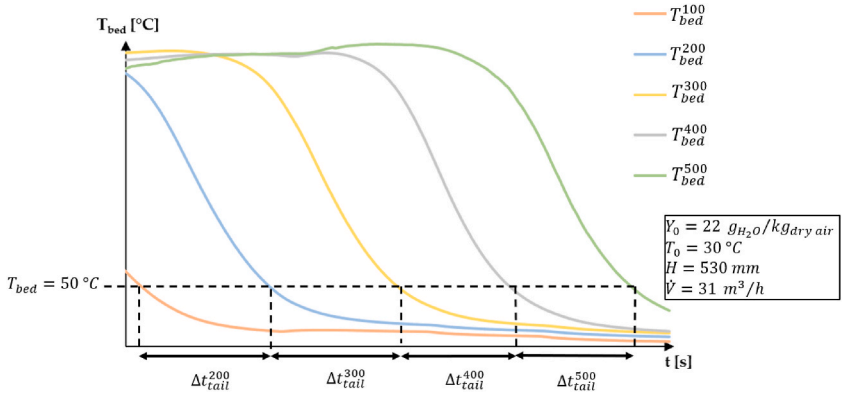


Fig. 9. Obtaining the time of the temperature decreases along the bed.

Table 6
Time of the temperature decreases along the bed

Parameter	100 mm	200 mm	300 mm	400 mm	500 mm
$t^h_{tail}\,[s]$	1056	2017	2967	3816	4689
$\Delta t^h_{tail}\,[s]$	N/A	961	950	849	873
$v^h_{tail}\left[\frac{mm}{s}\right]$	N/A	0.104	0.105	0.118	0.115

mixing, and heat transfer are ignored—the two velocities are equal, in which case $\frac{\bar{v}_{tail}}{\bar{v}_{front}} = 1$, consequently H^{tm}_{UNB} is equal to zero.

In the case studied, the temperature of the bed rose to $\sim 120°C$ during the process, so we cannot speak of ideal conditions or negligible heat transfer, as a result $\frac{\bar{v}_{tail}}{\bar{v}_{front}} = 0.146$. In practice, this is where the CWF's disadvantage of causing significant zone widening becomes apparent. The presumed mechanism behind the low v_{tail} resulting from the co-moving temperature and concentration fronts, and the resulting zone widening, can be described.

The CWF front reaches the particle at ambient temperature, where the adsorption process starts. Adsorption raises the temperature of the particles through an exothermic process to $T_{bed,max}$. Fewer water molecules can be adsorbed onto high-temperature adsorbent particles. As saturation occurs at this higher temperature, adsorption stops and the adsorption of water vapour is taken over by the clean particles located above.

If there is no adsorption, there is no heat generation either. The fed cold air stream (in this case, the particle temperature is $120°C$, while the temperature of the fed air is $30°C$) begins to cool the particle, causing its temperature to drop. At lower temperatures, however, the adsorbent's capacity increases, so adsorption resumes. Although this also generates heat, it is no longer sufficient to reheat the particle to the $T_{bed,max}$ value. This is followed by another slight drop in temperature, which frees up additional capacity. This process continues until the bed cools back down to the feed temperature. Thus, if the process is carried out until the outlet temperature

equals the inlet temperature, the bed will still contain the same amount of water $\left(X_{eq}^{T_0}\right)$, as at the feed temperature. However, if the adsorption process is carried out only up to the breakthrough point t_b, the length of the section that has not yet had time to cool down will be significant. The adsorbent at this section can only bind a smaller amount of water due to the higher temperature, which can be quantified by the calculated H_{UNB} value.

3.3. Evaluation of the pictures taken by thermal imaging camera

Thermal images were taken of the measurement described above, showing the temperature profile of the adsorber at various points in time. Fig. 10 shows the images after scale correction; note that the time intervals between the capture of each image are not identical.

Fig. 10 shows that the initially narrow adsorption zone widens and then slowly leaves the column. As the zone moves upward, the lower bed regions begin to cool back down to the feed temperature. This cooling process occurs more slowly as it moves upward along the bed.

The propagation and trailing velocities of the zone can also be calculated using thermal imaging data. By drawing a straight line connecting the bottom and top of the warm zones shown in Fig. 10, the slope of this line gives the values of v_{front} and v_{tail}. The ambient temperature in case of the measurement was $22°C$, therefore, the scale has been set so that the green zones begin at a temperature $10\ °C$ higher, at $32°C$. This results in the sharp boundary line visible in Fig. 10 at both the beginning and end of the zone. The distance of the boundary lines from the feed point could be measured by using image editing software. The height of the bottom and top of the zone, as well as the total height of the bed was measured in case of every thermal image, as shown in Fig. 11. Since it is known that $H = 530\ mm$ in reality, the values of h_{tail} and h_{front} could be calculated using proportionality.

The t time values at which the images were taken are known, so a data series $t - h_{front}$ and $t - h_{tail}$ values were generated. For this measurement, the data set is shown in Table 7.

We fitted straight lines to the data series shown in Table 7 using linear regression, as illustrated in Fig. 12.

In Fig. 12, the height of the front of the adsorption zone is shown in red as a function of time, while the height of the trailing end is shown in blue. The slope of the line fitted to the data points gives the values of v_{front} and v_{tail} respectively. The adsorption isotherm is nearly linear, so it could be assumed, that the concentration front propagates through the adsorber column at a constant velocity.

Since we have observed that the concentration front and the temperature front propagate together as a CWF in this system, the temperature front detectable by the thermal camera also moves at a constant velocity over time. However, this is only true for the examined bed. It is possible that the simplifications made when deriving equation (5), which defines the velocity, will significantly affect the velocity in the case of a considerably longer bed, so the velocity may not be constant along a greater length. In this case, the assumption that the velocities are constant is supported by the high R^2 values for both v_{front} and v_{tail} as well.

The value of v_{front} was calculated to be $0.718\ mm/s$, and the value of v_{tail} was $0.107\ mm/s$. Using these two velocity values, $t_b^{tc} = 738\ s$ was calculated using equation (20), which was also used for thermometers, and $H_{UNB}^{tc} = 451\ mm$ was calculated using equation (23).

In order to be able to investigate the accuracy of the three measurement methods, another measurement at a different operating point was taken. For this measurement, the feed flowrate was lowered to $26\ m^3/h$, the T_0 feed temperature was also lowered to $23\ °C$. Due to the decrease in the saturation temperature, the Y_0 concentration was also lower, $18\ g_{H_2O}/kg_{dry\ air}$. Due to the overall smaller feed load, the breakthrough time was significantly longer ($t_b^{br} = 1459\ s$). However, the length of the unused bed remained nearly the same ($H_{UNB}^{br} = 382\ mm$) suggesting that the value of the H_{UNB} is nearly independent from the operating parameters. The results obtained from both measurements are shown in Table 8.

3.3.1. Comparison of the three evaluation methods

Table 8 shows that the t_b values calculated using the three different methods do not differ significantly from one another. The value determined from the breakthrough curve can be considered the mean value, since the measured concentration increase at the outlet marks the actual breakthrough. The values obtained from the thermal methods approximate this value quite accurately, with the built in thermometers being slightly more accurate.

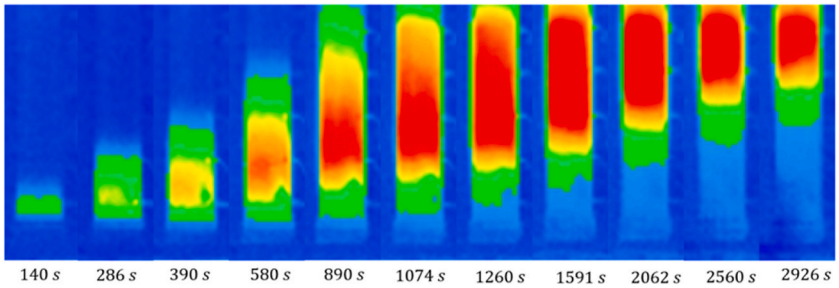


Fig. 10. Thermal images of the adsorber column.

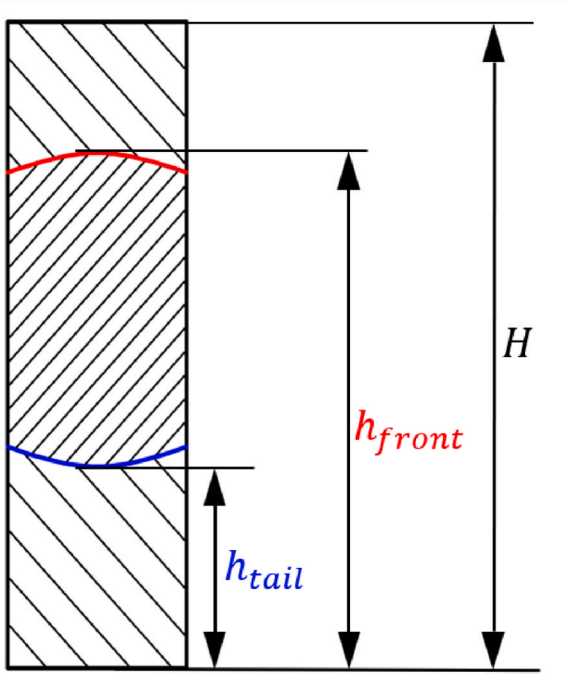


Fig. 11. Height measurement method in a thermal image.

Table 7
Values obtained from thermal images

t [s]	h_{front} [mm]	h_{tail} [mm]
0	0	N/A
140	96	N/A
286	202	N/A
390	283	N/A
580	413	N/A
1260	N/A	100
1591	N/A	136
2062	N/A	180
2560	N/A	235
2926	N/A	281

In case of H_{UNB} a "standard" method can not be chosen unless the level of saturation in the actual adsorbent particles are investigated. However, the most common method in literature for calculating H_{UNB} is the numeric integration of the breakthrough curve. As a result this method is considered as the mean value and the standard deviations shown in Table 8 are calculated compared to the breakthrough curve.

The thermal methods estimate the H_{UNB} with a greater error but they have a maximum error of 10%.

Minor errors arise from the instruments' internal errors and, in the case of the breakthrough curve, from the inaccuracies of numerical integration. An additional source of error is the time delay caused by the thermal resistance of the adsorber wall during the thermal imaging analysis. Table 9 summarizes the advantages and disadvantages of the three methods.

The built in thermometers can be designed into a new adsorber column and if necessary, can be built into an existing system as well. In processes, where the feed flowrate or concentration is not constant, they can be quite useful. The feed flowrate can be lowered in time if the operators see that the adsorption zone moves through the column too quickly. It is possible to predict, when the breakthrough will happen, which would not be possible by measuring the outlet concentration only.

The method based on the thermal imaging camera can be used to monitor existing columns where it would be complicated to build in thermometers. However, obtaining of real time data in this case is not possible due to the evaluation method. It is mainly suitable for development purposes, for example taking images of a column while in operation and then determining H_{UNB}. If it turns out to be too long, measures can be taken to reduce this length thus making the adsorption process more effective.

From an industrial design perspective, breakthrough time (t_b) dictates cycle switching schedules and prevents slippage, whereas the length of unused bed (H_{UNB}) governs bed overdesign and total adsorbent inventory. In our column, an uncertainty of $\sim 9-10\%$ in estimating H_{UNB} corresponds to an absolute bed height uncertainty of only $\sim 35-40$ mm in a 530 mm column. Because commercial

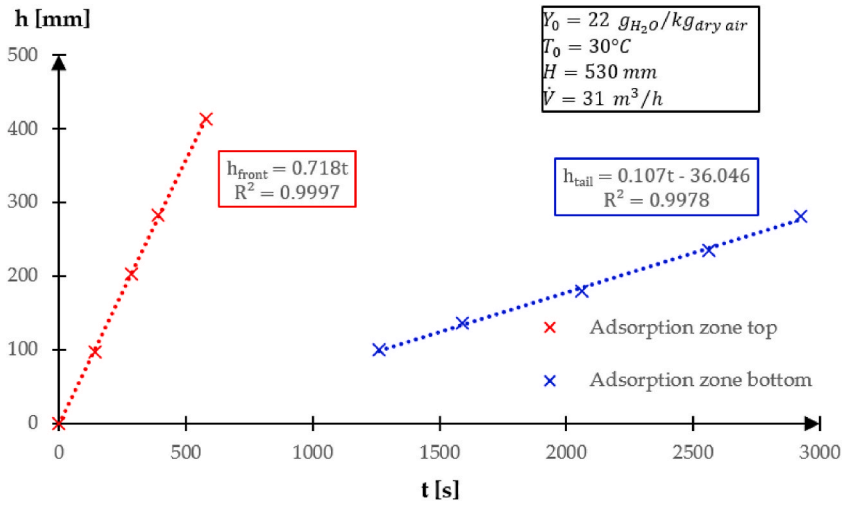


Fig. 12. Calculating the velocity of the front and bottom.

Table 8
Summary of measurement results

Operating parameters	Parameter	Break through curve	Thermometer	δ_{tm} [%]	Thermal imaging camera	δ_{tc} [%]
$\dot{V} = 31m^3/h$ $T_0 = 30°C$ $Y_0 = 22g_{H_2O}/kg_{dry\ air}$	$t_b\ [s]$ $H_{UNB}[mm]$	720 413	701 453	*2.6* *9.6*	738 451	*2.5* *9.2*
$\dot{V} = 26\ m^3/h$ $T_0 = 23°C$ $Y_0 = 19g_{H_2O}/kg_{dry\ air}$	$t_b\ [s]$ $H_{UNB}[mm]$	1459 382	1476 422	*1.1* *10*	1510 386	*3.5* *1.0*

Table 9
Comparison of the measurement methods

Methods	Advantages	Disadvantages
Breakthrough curve	Easy to evaluate; Well established	No real time data available due to the significant time constant
Thermometer	Easy to evaluate v_{front} and v_{tail} can be determined at different heights→non-linear behaviour can be considered	Thermometers need to be built into the adsorbent bed
Thermal imaging camera	No need for in-built sensor	Evaluation is time consuming

fixed-bed adsorbers are routinely designed with safety margins of $15-25\%$ to accommodate adsorbent aging, flow maldistribution, and feed variations, an estimation error under 10% via thermal tracking falls well within acceptable engineering tolerances.

Regarding scale-up, certain limitations must be considered. In large-scale industrial adsorbers, opaque metal walls and heavy external insulation prevent direct thermal imaging of the bed. Furthermore, large bed diameters may lead to radial temperature and velocity non-uniformities that cannot be detected by exterior surface observations alone. Consequently, while thermal imaging serves as a non-intrusive diagnostic tool for transparent or pilot-scale units, internal multi-point resistance thermometer lances represent the most viable and direct scale-up approach for industrial monitoring.

4. Summary

In our study, we investigated the thermal effects occurring during the adsorption of water vapor on zeolite particles under adiabatic conditions in a fixed-bed adsorber column. Due to the exothermic nature of the adsorption process, the zeolite bed gradually heats up as the adsorption zone propagates. A concentration front and a temperature front form along the length of the bed; their velocities are not always the same, it depends on material properties and operating parameters.

Using the measuring equipment we built, the temperature of the adsorbent was recorded as a function of time during the adsorption

process at multiple heights simultaneously, and thermal images were also taken of the operating adsorber. In addition to measuring changes in temperature, the breakthrough curve, as well as the temperature and flow rate of the inlet gas, were also recorded.

The evaluation confirmed that, in the system we built, the concentration and temperature fronts propagate together. The breakthrough time of the adsorber and the length of the unused bed remaining at the end of the operation were determined using three methods: by integrating the breakthrough curve, using thermometers built into the bed, and from a series of thermal images. The breakthrough curve method can be considered a reference, since in practice t_b and H_{UNB} are most often determined this way. Compared to this, the relative error of the value calculated using the built-in thermometers had a maximum deviation of 2.6%, while this deviation was 3.5% when using thermal camera images. The length of the unused bed section was also determined from the breakthrough curve; compared to this, we obtained results with a maximum relative error of 10% using thermometers and 9.2% using a thermal imaging camera.

The results obtained confirmed that, in adiabatic cases, analysing temperature changes also allows for the determination of the breakthrough time and the length of the unused bed. This is useful in cases where, for some reason, it is not possible to measure the exact outlet concentration. It is also possible to determine exactly where the adsorption zone is located at a given time, which would be impossible by analysing just the outlet concentration. The advantage of built-in thermometers is their high accuracy, while the advantage of using thermal imaging camera is that no modifications to existing equipment are required to take measurements.

CRediT authorship contribution statement

Levente Sor: Writing – original draft, Visualization, Validation, Investigation, Data curation, Conceptualization. **Tibor Poós:** Writing – review & editing, Supervision, Software, Resources, Funding acquisition, Conceptualization, Writing – original draft, Project administration, Formal analysis.

Fundings

This work was supported by the János Bolyai Research Scholarship of the Hungarian Academy of Sciences (BO/00059/23/6) and by the Hungarian Scientific Research Fund (NKFIH FK-142204).

Declaration of competing interest

The authors declare that they have no known competing financial interests or personal relationships that could have appeared to influence the work reported in this paper.

Nomenclature

A	Cross sectional area of the adsorber column	m^2
C	Outlet adsorptive concentration	kg/m^3
c_p	Specific heat	J/kgK
d	Diameter of orifice flange	m
g	Standard acceleration due to gravity (9,81)	m/s^2
h	Distance from the feed point	m
H	Full height of the adsorbent bed	m
L	Water level in the U pipe manometer	m
p	Pressure	Pa
M	Molar mass	g/mol
R	Universal gas constant (8,314)	$J/(kmol)$
T	Temperature	$^\circ C$
t	Elapsed time	s
v	Flow velocity relative to the open cross-sectional area	m/s
X	Adsorbate concentration/water content of the adsorbent	kg_{H_2O}/kg_{dp}
Y	Absolute humidity	$kg_{H_2O}/kg_{dry\ air}$

Greek letters

α	Flow coefficient	1
Δ	Change in the given parameter	1
ε	Porosity	1
ε_{exp}	Expansion coefficient	1
φ	Relative humidity	1, %
ρ	Density	kg/m^3
δ	Relative error	%

Subscripts and Superscripts

*	Equilibrium vapor pressure
0	Inlet
ads	Adsorbent
air	Air
b	Breakthrough
bed	Bed
br	Calculated based on the breakthrough curve
bulk	Bulk
eq	Equilibrium
fl	Orifice flange
front	Top of the adsorption zone
gas	Gas phase
h	Time constant of a sensor
H_2O	Water
rec	Recorded
start	Start of the measurement
tail	Bottom of the adsorption zone
tc	Calculated based on thermal images
temp	Temperature
tm	Calculated based on in-built thermometers
u	Proportional to the useable capacity
UNB	Unused

Data availability

Data will be made available on request.

References

[1] D.M. Ruthven, S. Farooq, Air separation by pressure swing adsorption, Gas Sep. Purif. 4 (3) (Sep. 1990) 141–148, https://doi.org/10.1016/0950-4214(90)80016-E.

[2] 'Activated carbon as an adsorbent for CO2 capture: adsorption, kinetics, and RSM modeling | ACS Omega | ACS Publications'. Accessed: September. 17, 2026. [Online]. Available: https://pubs.acs.org/acsodf/article/9/2/2080/1554870/Activated-Carbon-as-an-Adsorbent-for-CO2-Capture.

[3] K.C. Ng, K. Thu, Y. Kim, A. Chakraborty, G. Amy, Adsorption desalination: an emerging low-cost thermal desalination method, Desalination 308 (Jan. 2013) 161–179, https://doi.org/10.1016/j.desal.2012.07.030.

[4] T. Poós, Determination of adsorption and desorption isotherms of zeolite LTA (4A) by gravimetric method, Dry. Technol. 0 (0) (Dec. 2025) 1–11, https://doi.org/10.1080/07373937.2025.2606969.

[5] Performance evaluation of a single-stage two-bed adsorption chiller with desalination function', Scilit. Accessed: September. 16, 2026. [Online]. Available: https://www.scilit.com/publications/a7f1e73a330d07b2bf223e530bb7de31.

[6] W. L. McCabe, J. C. Smith, and P. Harriott, Unit Operations of Chemical Engineering. McGraw-Hill Inc.

[7] M.a.S.D. Barros, P.A. Arroyo, E.A. Silva, M.a.S.D. Barros, P.A. Arroyo, E.A. Silva, General aspects of aqueous sorption process in fixed beds, in: Mass Transfer - Advances in Sustainable Energy and Environment Oriented Numerical Modeling, IntechOpen, 2013, https://doi.org/10.5772/51954.

[8] T. Kundu, L. Gilmanova, W.F. Yong, S. Kaskel, Metal-organic frameworks for environmental applications, in: J.C. Moreno-Piraján, L. Giraldo-Gutierrez, F. Gómez-Granados (Eds.), Porous Materials: Theory and Its Application for Environmental Remediation, Springer International Publishing, Cham, 2021, pp. 1–39, https://doi.org/10.1007/978-3-030-65991-2_1.

[9] D.M. Routheven, Principle of Adsorption and Adsorption Processes, University of, Wiley-Interscience Publication, New Brunswick, Fredericton, 1984.

[10] T. Poós, E. Varju, Determination of mass transfer zone at adsorption process, EXPRES (2020) 73–78.

[11] E. Ivanova, M. Kosatava, G. Stefanov, Temperature profiles during adiabatic fixed bed adsorption of water and organic vapours on zeolite 4A, Ournal Univ. Chem. Technol. Metall. 44 (4) (2009) 71–378.

[12] D. Basmadjian, The Little Adsorption Book: a Practical Guide for Engineers and Scientists, CRC Press, Boca Raton, 1996.

[13] Laborrendszer, Laboratóriumi Információs Rendszer, LIMS'. Accessed: March. 4, 2026. [Online]. Available: https://www.interconnect.hu/index2_hu.php.

[14] EngineerExcel, 'Orifice Meter Working Principles and Applications', EngineerExcel. Accessed: April. 26, 2026. [Online]. Available: https://engineerexcel.com/orifice-meter/.

[15] P. Mizsey, *Folyamatirányítási Rendszerek*. Budapest: Budapesti Műszaki És Gazdaságtudományi Egyetem, 2011.

[16] A.L. Buck, New equations for computing vapor pressure and enhancement factor, J. Appl. Meteorol. 20 (Dec. 1981) 1527–1532, https://doi.org/10.1175/1520-0450(1981)020%3C1527:NEFCVP%3E2.0.CO;2.

[17] Abraham Savitzky, M.J.E. Golay, Smoothing and differentiation of data by simplified least squares procedures, Anal. Chem. 36 (8) (Jul. 1964) 1627–1639, https://doi.org/10.1021/ac60214a047.

[18] L. Qiu, V. Murashov, M.A. White, Zeolite 4A: heat capacity and thermodynamic properties, Solid State Sci. 2 (8) (Dec. 2000) 841–846, https://doi.org/10.1016/S1293-2558(00)01102-X.

[19] Dry and Humid Air - specific heat capacity, in: https://powderprocess.net/Tools_html/Air/Air_Humid_Specific_Heat.html. (Accessed 8 April 2026).